

An Investigation of Cloud Cavitation about a Sphere

P.A.Brandner¹, G.J. Walker², P.N. Niekamp¹ and B. Anderson³

¹Australian Maritime Hydrodynamics Research Centre
Australian Maritime College, Tasmania, 7248 AUSTRALIA

²School of Engineering
University of Tasmania, Hobart, Tasmania, 7001 AUSTRALIA

³Maritime Platforms Division
Defence Science and Technology Organisation, Fishermans Bend, Victoria, 3032 AUSTRALIA

Abstract

Cloud cavitation occurrence about a sphere is investigated in a variable pressure water tunnel using still and high-speed photography. The model sphere, 0.15 m in diameter, was sting mounted within a 0.6 m square test section and tested at a constant Reynolds number of 1.5×10^6 with cavitation numbers varying between 0.36 and 1.0. High-speed photographic recordings were made at 6 kHz for several cavitation numbers. Shedding phenomena and frequency content is investigated by means of pixel intensity time series data using wavelet analysis.

The boundary layer at cavity separation is shown to be laminar for all cavitation numbers, with Kelvin-Helmholtz instability the main mechanism for cavity break up and cloud formation at high cavitation numbers. At intermediate cavitation numbers, cavity lengths allow the development of re-entrant jet phenomena providing a mechanism for shedding of large scale Karman-type vortices similar to those for low mode shedding in single-phase subcritical flow. This shedding mode is eliminated at low cavitation numbers with the onset of supercavitation.

Introduction

Cloud cavitation is a general term for unsteady or periodic cavitation phenomena occurring about a body involving formation, detachment and collapse of sheet cavities. The collapse or condensation of the shed cavity in the wake of the body forms 'cloud' like structures. Due to the unsteady nature of cloud cavitation it has various consequences for hydraulic and marine equipment including problems of unsteady flows, noise/vibration and cavitation erosion. Through the use of modern experimental diagnostics and computational fluid dynamics significant insights have been gained into the complex physics involved. However, despite these advances there remains much to be understood and cloud cavitation continues to be an area of ongoing research.

Most investigation has been directed to cloud cavitation associated with lifting surfaces or hydrofoils as well as internal flows, Brennen [5], Franc and Michel [8] and Schnerr et al. [15]. The occurrence of cloud cavitation in such flows may involve several mechanisms. Brennen [5] refers to the coherent nature of this cloud cavitation as being due to natural instabilities or externally imposed flow fluctuations and more recently by Franc and Michel [9] and Franc [8] in detailed reviews as due either to intrinsic or system based instabilities. Franc and Michel [9] have investigated and reviewed extensive work on the role of unsteady cavity closure and re-entrant jet formation in cloud cavitation as an intrinsic instability. System based instabilities are referred to as those due to interaction of sheet cavities with hydraulic circuits of water tunnels or between those of neighbouring blades

of turbomachinery. In addition to re-entrant jet formation, the role of surface tension in the contact between the sheet cavity and re-entrant jet in cloud cavitation formation has been investigated by Mørch et al. [13]. Shock wave phenomena in cloud cavitation have been also investigated numerically by Riesman et al. [14] and Schnerr et al. [15].

Despite the extensive literature there appears to be little work on cloud cavitation for bluff body flows. Typical examples of which may include ventilated and natural cavity formation about sonar domes and other bluff appendages of surface and undersea vehicles. The present investigation was therefore conceived as a preliminary study of cloud cavitation about bluff bodies and to test experimental methods. Given the extensive work on single-phase flow about spheres this was chosen as a starting point.

Single-phase unsteady flow phenomena in sphere wakes have recently been reviewed by Bakić & Perić [3]. Above $Re \approx 10^3$ there are two modes (high and low) of regular vortex shedding. These phenomena have been observed on both wind and water tunnel facilities using hot-wire anemometry, and visualisation with smoke and dye injection assisted by laser light sheet illumination. The low mode, with Strouhal number $S_K \approx 0.2$, corresponds to large-scale Karman vortex shedding. The large-scale vortices have a horseshoe structure, and rotate irregularly around the longitudinal axis of the sphere flow. While local observations may sometimes give the impression of helical vortex structures in the wake, there is no evidence for their existence (which would, in any case, violate Thomson's circulation theorem).

The high mode unsteadiness is generated by Kelvin-Helmholtz instability in the separating laminar shear layer. The corresponding Strouhal number, S_H , varies as about the 0.7 power of Reynolds number. Bakić & Perić found $S_H = 0.0039 Re^{0.695}$ for $22,000 < Re < 400,000$. There is no evidence for this high frequency unsteadiness causing discrete vortex shedding behind a sphere.

Above the upper critical Reynolds number ($Re \approx 4 \times 10^5$ with free-stream turbulence level about 0.5%, as in the present investigation) periodic vortex shedding can no longer be detected in single-phase flow. In the supercritical regime defined by Achenbach [1] the unstable separated shear layer undergoes transition to turbulence and reattaches to form a laminar separation bubble; the turbulent boundary layer thus formed subsequently separates at about 120° from the forward stagnation point. With increasing Reynolds number the separation bubble gradually disappears, leading to the transcritical flow regime beyond $Re \approx 1.5 \times 10^6$ where boundary layer transition occurs upstream of the pressure minimum on the sphere.

In cavitating flows the visualisation of flow phenomena is facilitated by the presence of the gas/vapour cavities. Vortex structures can easily be identified from the generation of new bubbles within the low-pressure vortex cores, or by the entrainment of bubble clouds into the vortical flow regions. Where large cavities form, it is possible to identify wave phenomena in the shear flow adjacent to the cavity boundary from perturbations of the interfacial surface. Kelvin-Helmholtz instability of the shear layer separating from a cavitating sphere causes transverse flow perturbations that are restrained by surface tension; this produces regular waviness of the interfacial surface that can readily be seen with glancing illumination.

Advances in still and high-speed digital photography provide significant opportunities for the observation and analysis of unsteady cavitation phenomena. In the present investigation these techniques have been used to investigate cloud cavitation about a sphere in a cavitation tunnel. The relatively high spatial resolution of still photography enables small scale phenomena associated with cavity formation to be discerned. The temporal resolution of the high-speed photography enables the global character and frequency content of the cloud cavitation to be analysed. With suitable lighting the time series of individual or spatially averaged pixel intensity may be used for frequency analysis. For the present investigation this has been carried out using wavelet analysis. These techniques have been extensively used in the investigation of various turbulent flow phenomena including cloud cavitation, Kjeldsen and Arndt [12]. Reviews have been presented by Farge [7] and Jaffard et al. [11] with practical techniques presented by Torrence and Compo [16] and Addison [2].

Experimental Overview

All tests were performed in the Australian Maritime College Tom Fink Cavitation Tunnel, a closed recirculating variable pressure water tunnel. The test section dimensions are 0.6m x 0.6m cross section x 2.6m long. The velocity may be varied from 2 to 12m/s and the centreline static pressure from 4 to 400 kPa absolute. Studies may involve the investigation of steady and unsteady flows, two-phase flows including cavitation, turbulence and hydro-acoustics. Details of the tunnel setup and operation are given in Brandner et al. [4].

The 0.15 m diameter smooth PVC sphere was located midway along the test section on the longitudinal axis supported by a sting mount as shown in Figure 1. Testing was carried out at a constant Reynolds number of 1.5×10^6 which is around the lower limit of the transcritical flow regime in single phase flow defined by Achenbach [1]. Cavitation numbers varied between 1.0 and 0.36. The Reynolds number is defined as $Re = UD/\nu$ and the cavitation number as $\sigma = (p - p_v)/\frac{1}{2}\rho U^2$ where U is the freestream velocity, D the sphere diameter, p the test section static pressure at the sphere centre, p_v the vapour pressure and ρ the fluid density. Dissolved oxygen content of the tunnel water was maintained at approximately 1.2 ppm.

Still photography was carried out using a Canon EOS 300D 35mm SLR digital camera (3072x2048 image resolution) and EF-S 18-55mm f/3.5-5.6 lens with triggered stroboscopic lighting (DRELLO 1018/LE4040). High speed photography was carried out using a LaVision HighSpeedStar5 camera with Nikkor 55mm, f/1.4 lens controlled using DaVis 7.1.3 software with lighting from a dedolight DLH650. The camera uses a 10-bit CMOS sensor and was operated at a frame rate of 6 kHz and resolution of 1024x512 with 4096 images recorded for all cavitation numbers investigated. With appropriate lighting, image intensity was found to be useful for identifying various flow features such as the growth of reforming sheet cavities,

transition in the interfacial layer, and cavity break-up and cloud formation, as shown in Figure 1.

Time series of individual pixel intensities were found to have substantial high frequency noise from fine scale cavity surface features. An effective means of filtering the time series is spatial averaging within the scale of the structures desired to be resolved. A region of 10 x 25 pixels was found to provide sufficient spatial resolution and reduce undesirable noise. For all cavitation numbers tested it was found that time series resolving all features of interest, for the 10 x 25 region, could be taken from a single location centred on pixel 275, 210 as shown on Figure 1. The time series for each cavitation number were examined using wavelet analysis to investigate frequency content and coherence of cloud cavitation phenomena. The wavelet analysis method of Torrence and Compo [16] was used, i.e. a continuous wavelet transformation in Fourier space, using in this case a DOF (derivative of a Gaussian) order 2 wavelet.

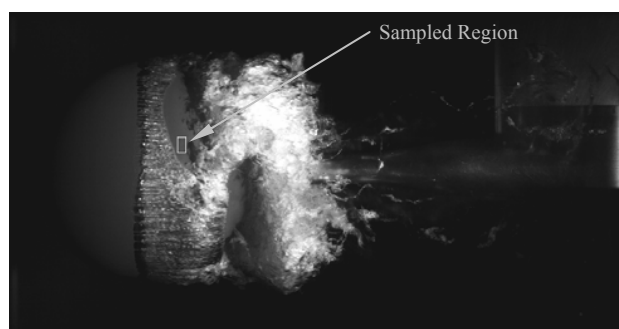
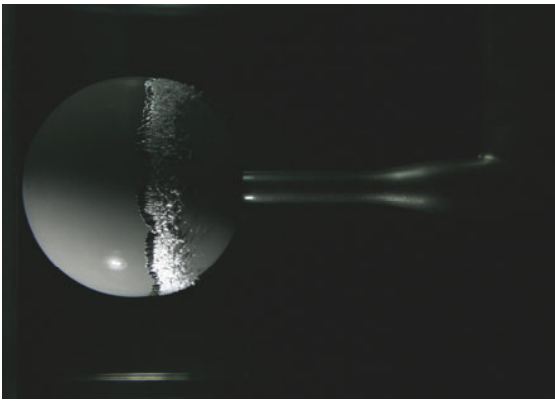


Figure 1. Image from high-speed photography of cavitating sting mounted sphere located on test section longitudinal axis. Sampled region of 10 x 25 pixels centred at 275, 210 indicated.

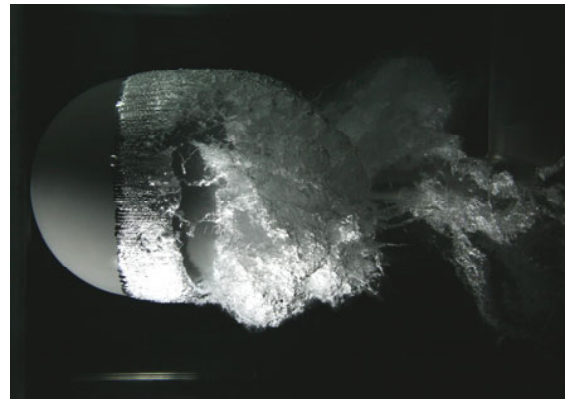
Results

A series of still photographic images of cavitation occurrence about the sphere, for several cavitation numbers, is shown in Figure 2. Cavitation inception was observed to occur at σ of about 1.0, corresponding to the supercritical minimum pressure coefficient of -1.1 . The cavity thus formed is stable and of $0.15D$ approximate length, as shown in the first photograph of Figure 2. Due to the large range of cavitation numbers investigated, low dissolved gas content was used to minimise the presence of large bubbles at the lower cavitation numbers. As a result of this, hysteresis was observed at inception due to lack of nuclei, with a higher 'desinent' cavitation number required to eliminate the sheet cavity after inception. With reduction of the cavitation number to 0.95 the sheet cavity became unstable, initiating cloud cavitation. Cloud cavitation was observed to occur between σ values of 0.95 and 0.4, as shown in Figure 2. Below a σ of 0.4, re-entrant jet phenomena no longer promoted large scale break-up of the cavity; and hence the formation of super-cavitation at a σ of 0.36, as shown in Figure 2.

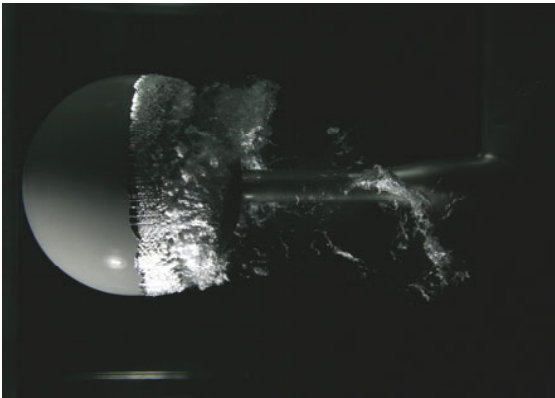
The location of the cavity leading edge varies linearly from 97° to 72° from the sphere front stagnation point for σ values from 1.0 to 0.36 respectively. These results are consistent with those presented by Brennen [5] for varying Reynolds numbers, cavitation numbers and tunnel blockage ratios. However, they differ significantly from data for single phase flow. Achenbach [1] reports separation from a smooth sphere at about the same turbulence intensity (around 0.5%) varying from 83° for subcritical flow (up to $Re = 2 \times 10^5$) to 120° for supercritical ($Re = 3 \times 10^5$), and remains approximately constant above and below these Re values.



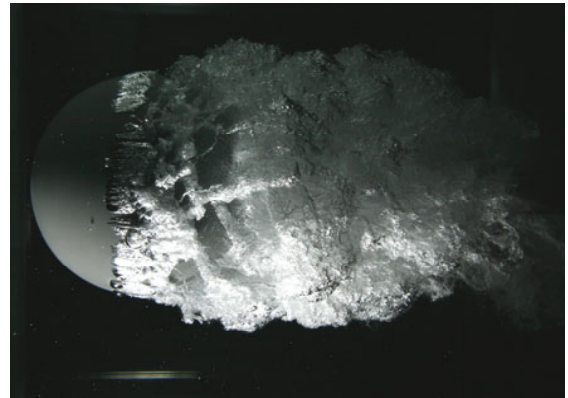
$\sigma = 1.0$



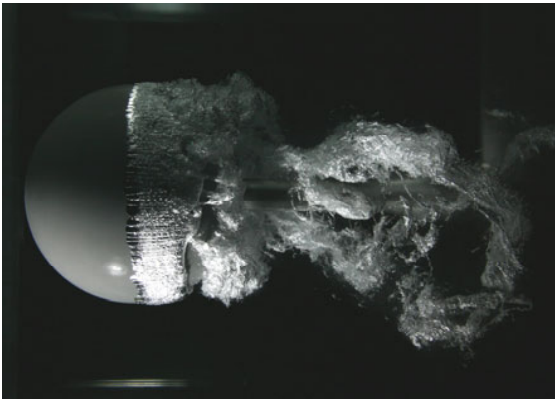
$\sigma = 0.6$



$\sigma = 0.9$



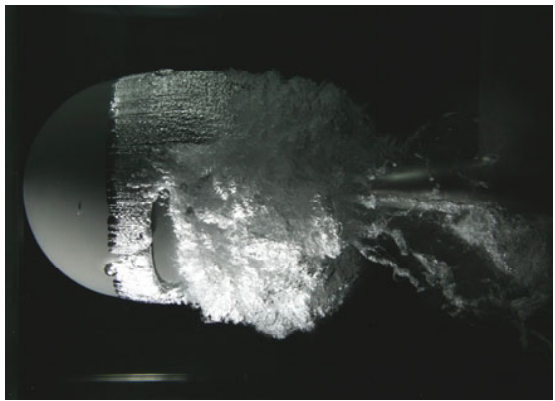
$\sigma = 0.5$



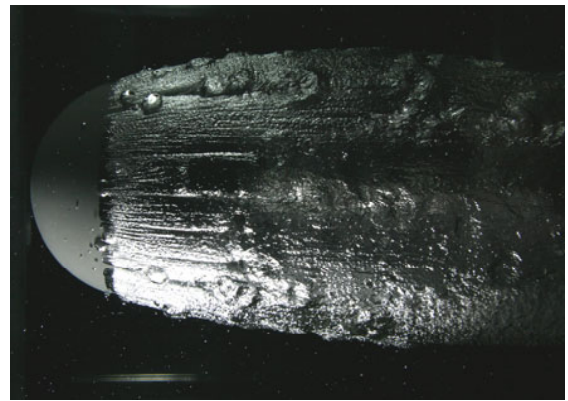
$\sigma = 0.8$



$\sigma = 0.4$



$\sigma = 0.7$



$\sigma = 0.36$

Figure 2. Still photography of cavitation occurrence at several cavitation numbers

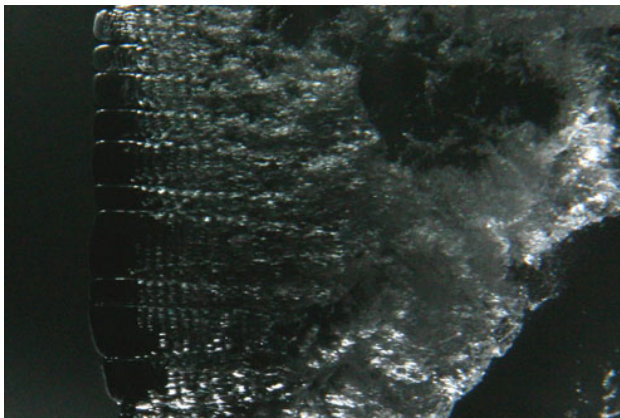


Figure 3. Typical cavity leading edge structure of laminar cells with circumferential K-H instability waves and superimposed streamwise vortex structures (cavitation number of 0.9).

For all cavitation numbers the structure of the cavity leading edge is complicated by viscous and surface tension effects as shown in Figure 3. The cavity separation is typical of that associated with laminar boundary layer separation, as described by Franc and Michel [9] and Brennen [5]. The cavity leading edge is convex due to surface tension effects with the laminar nature of the separated shear layer apparent from the glassy cavity surface. The location of the cavity separation is determined by the pressure distribution of the combined wetted flow and separating cavity. As noted by Franc and Michel the location of the laminar separation, and indeed its existence, may differ significantly from the case of fully wetted flow. Due to the requirement for an adverse pressure gradient for boundary layer separation the pressure ahead of the cavity is actually lower than the cavity pressure. Hence entrained nuclei may be activated near the pressure minimum, forming large bubbles that temporarily break up the sheet cavity leading edge as shown in some photographs of Figure 2.

Figure 3 shows the cavity leading edge to be structured in cells of approximately uniform circumferential spacing on each of which the initial laminar flow is destabilised with the formation of transverse waves. The division of the cavity leading edge into cells is most likely due to the convex shape of the cavity creating concave flow ahead of the leading edge whereby streamwise vortices form from Görtler-instability. The transverse waves on each cell are from Kelvin-Helmholtz (K-H) instability in the separating shear layer. The wavelength measured from the still photographs gives about 1.35 mm for all cavitation numbers. The frequency of the K-H waves for a σ of 0.9 measured from high-speed photography taken at a frame rate of 20 kHz is about 8 kHz. Ho & Huerre [10] give $f = 0.016 \bar{U} / \theta$ as the frequency for maximum K-H wave amplification. Using the surface pressure distribution data of Fage [6] for subcritical single-phase flow, the laminar boundary layer thickness θ at separation computed by Thwaites method with the Mangler transformation is estimated to be about 0.035 mm. Combining with $\bar{U} = U/2 \approx 6.5 \text{ m/s}$ at separation (where the cavity interfacial layer commences) gives $f \approx 6 \text{ kHz}$. This is in reasonable agreement with the observed frequencies, and provides strong evidence that the observed waviness of the interfacial layer is due to inviscid instability: the frequency of progressive capillary waves would be an order of magnitude higher.

The interfacial layer also shows streamwise streaks at two different scales. As discussed by Ho & Huerre [10], single-phase plane mixing layers exhibit spanwise-periodic streamwise streaks caused by secondary counter-rotating streamwise vortices

superimposed on the primary rolls generated by the K-H instability; the average spanwise spacing of these streaks is of the same order of magnitude as the local shear layer thickness. For the sphere flow investigated here the fine-scale streaks have a spanwise spacing of about a quarter of the streamwise (K-H) wavelength (or around 0.3 mm), and the estimated shear layer thickness at separation is about 0.25 mm : thus they appear compatible with the secondary flow mechanism observed in single-phase mixing layers. The larger scale streaks arise from circumferential waviness in the cavity boundary at separation, and appear associated with surface tension effects. Both forms of streakiness are probably caused by Görtler instability associated with locally concave flow curvature.

Turbulent breakdown of the interfacial layer and subsequent entrainment of gas/vapour bubbles appear to be the main mechanism of cavity break-up and bubble cloud formation for σ values of 1.0 and 0.95. The moderate cavity lengths developed between σ values of 0.9 and 0.4 allow the re-entrant jet phenomena to develop and dominate the cavity break-up with large scale vortex shedding and bubble cloud formation. For $\sigma < 0.4$ the cavity length becomes sufficiently long that the re-entrant jet no longer penetrates to the rear surface of the sphere and the super-cavitating flow regime occurs.

From the high-speed photography, a wavelet transformation of the time series derived from the spatially averaged pixel intensity of the region indicated in Figures 1 and 5 was carried out for σ values between 0.95 and 0.4. The wavelet power spectrum for each cavitation number, normalised to peak amplitude, is shown in Figure 4. The Strouhal number is, $S = fD/U$, where f is the wavelet characteristic frequency. It should be noted that the the upper cut-off frequency/Strouhal number is below that required to detect the K-H waves discussed earlier.

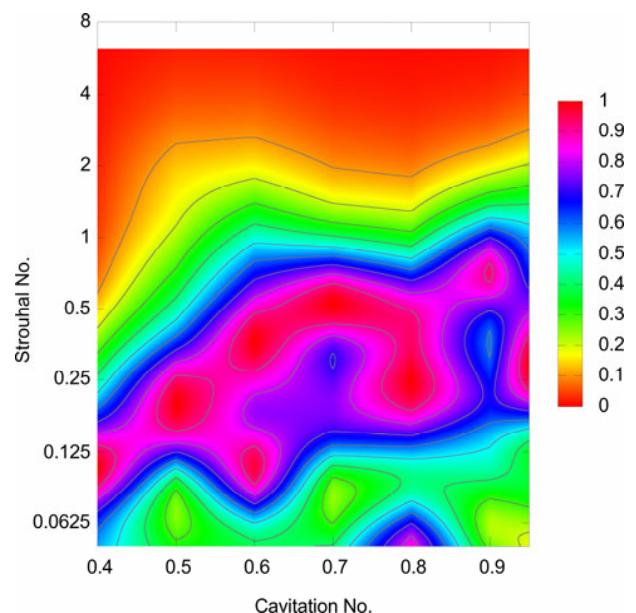
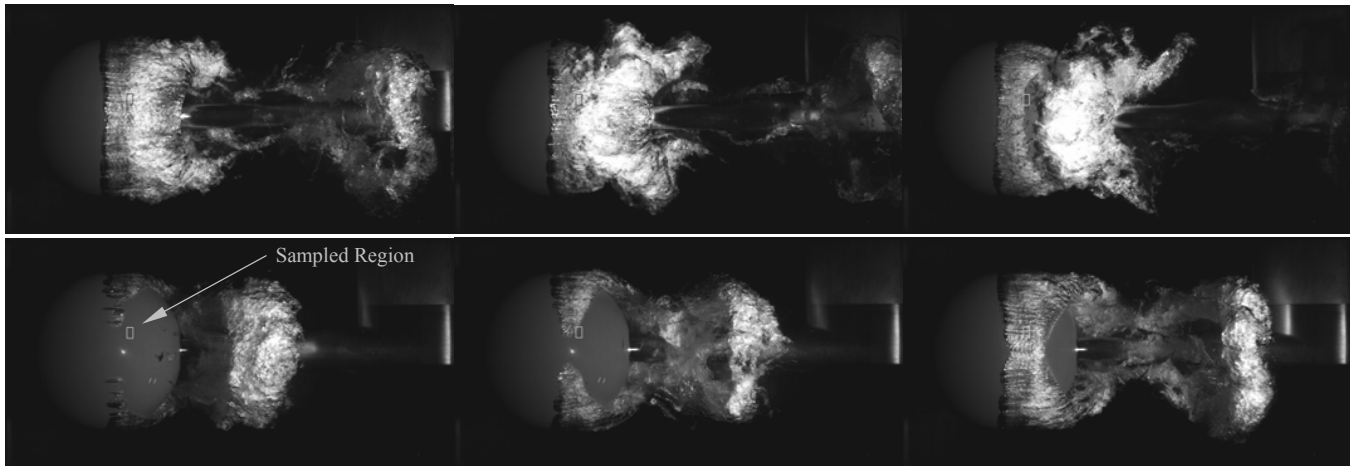
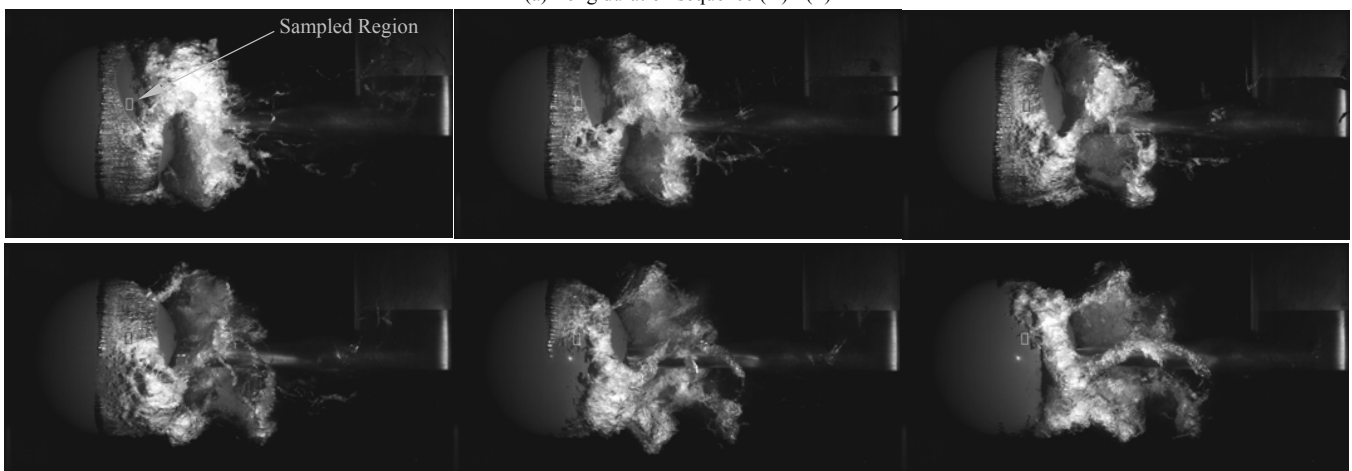


Figure 4. Normalised wavelet power spectrum as a function of cavitation number

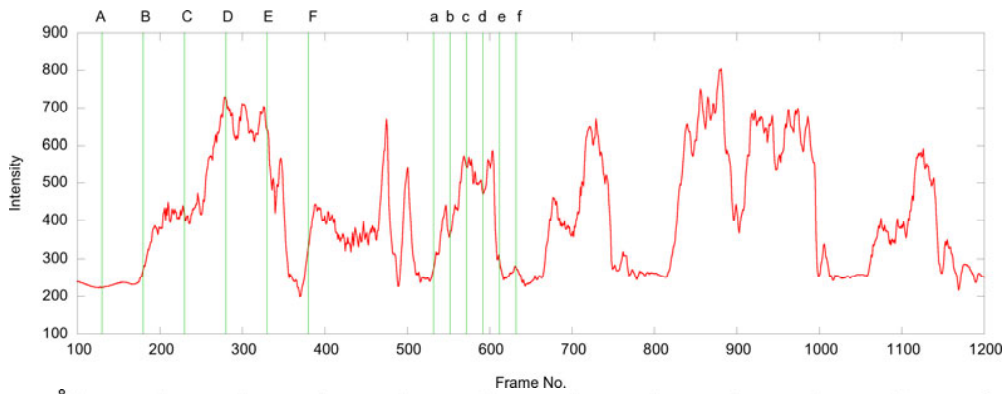
For $\sigma = 0.95$, the sheet cavity breaks down to cavitating vortex filaments of the scale of the interfacial instabilities described above. The filaments accumulate just downstream of the break-up area and are shed with a dominant frequency similar to non-cavitating sub-critical flow with a $S \approx 0.28$, as shown in Figure 4. The sheet cavity length fluctuates with trailing edge break-up and the shedding cloud but its leading edge remains in place virtually all the time.



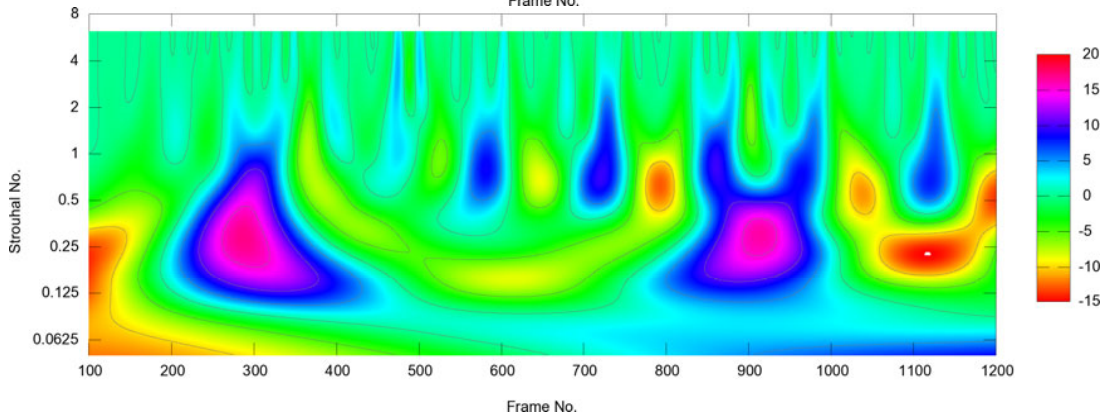
(a) Long duration sequence (A) - (F)



(b) Short duration sequence (a) - (f)



(c) Spatially averaged time series data for region indicated



(d) Wavelet transform plot for time series data in (c)

Figure 5 (a) sequences of long duration shedding events; (b) sequences of short duration shedding events; (c) spatially averaged time series data for region indicated in (a) and (b); (d) wavelet transform of plot for time series data in (c). Cavitation number 0.8.

At $\sigma = 0.9$, cavity lengths become sufficient for a re-entrant jet to form; this directly affects the break-up of the sheet cavity. Initial breakdown typically occurs at about mid cavity length, at several circumferential sites from which fronts emanate; the sheet cavity then breaks down to cavitating filaments as described above. The filaments either condense or are shed by advection with the vortical cloud. The formation and shedding of each cloud are closer to axisymmetric. Some cycles cause the sheet cavity to be displaced for large lengths of the circumference, but for only a short duration with the cavity quickly growing anew. The power spectrum has two peaks at S values of about 0.2 and 0.72. The duration of each event appears to depend on the cavity length and therefore the time required for sheet cavity growth and re-entrant jet return to affect cavity break up.

The cavitation behaviour at $\sigma = 0.8$ is similar to that at 0.9 except that maximum cavity lengths become greater and cavity formation and shedding show larger departures from axisymmetry. Shed cloud cavities and forming sheet cavities interact in a complex way, examples of which are given in Figure 5. Figures 5(a) and (b) shows image sequences of two shedding events on which the sampled region described earlier is depicted. Figures 5(c) and (d) show a segment of time series containing the above events and corresponding wavelet transformation of the spatially averaged image intensity time series data from the depicted region. Sequence A – F of Figure 5(a) shows the oblique shedding of a near complete vortical ring, except for a section that remains connected to the forming cavity on the far side of the sphere such that a hairpin like structure is shed. The high-speed photography suggests that following this event, a symmetric but less intense event occurs on the opposite side of the sphere. The event following this, sequence a – f in Figure 5(b), where cavity lengths are shorter shows an apparent helical coupling between shed and forming cavities. The time series data and wavelet analysis, segments of which are shown in Figure 5, show these modes to be typical and to characterise the two dominant frequencies in the power spectrum with S values of about 0.24 and 0.4. As shown in the image sequences of Figure 5 at a σ of 0.8, the shedding events are of sufficient intensity for large regions of the sheet cavity to be entirely displaced for significant periods of the shedding cycle.

Cavitation behaviour at σ values of 0.6 and 0.7 show similar coupling or modulation of forming cavities by those shed as for $\sigma = 0.8$ but with greater maximum cavity lengths and shed cavity volumes. For $\sigma = 0.7$ the peak frequencies of the power spectra correspond to S values of about 0.2 and 0.52; for $\sigma = 0.6$, the S values are about 0.11 and 0.35. Both these cavitation numbers are sufficiently low that, despite the intensity of the shedding events, the sheet cavity is displaced for only short periods of the shedding cycle.

At $\sigma = 0.5$, cavity lengths have grown to about two sphere diameters and the re-entrant jet behaviour is becoming predominant and tending more axisymmetric, causing nearly simultaneous break down of the entire sheet cavity circumference. Due to the almost simultaneous break down of the entire sheet cavity there is little interaction between shed clouds and newly growing sheet cavities, so that only one dominant frequency is present in the power spectrum shown in Figure 4. The presence of cavitating vortices within the interfacial layer can be seen at break down of the sheet cavity as is the case for larger cavitation numbers, but with much greater volume, as apparent in Figure 2. At break down a new sheet cavity is initiated almost immediately following closely ahead of the previously shed cloud.

For $\sigma = 0.4$ the cavity length becomes sufficient that the re-entrant jet barely reaches the sphere. The returning liquid/vapour mixture is mostly being carried back downstream as it impinges on the cavity wall. Due to the greater cavity volume and greater distance travelled by the re-entrant jet there is sufficient time for the jet fluid to fall due to gravity. With the plunging of the re-entrant jet fluid only the bottom of the sheet cavity is affected. With most of the fluid being carried downstream as it impinges on the lower half of the sheet cavity, the often observed ‘breaking wave’ type cavity closure occurs. Occasionally sufficient re-entrant jet fluid accumulates to cause a short break down of the sheet cavity hence the frequency with an S value of about 0.1 shown in Figure 4.

In summary, for high cavitation numbers just below inception break down of the cavity is due mainly to instabilities within the interfacial layer resulting in predominantly axisymmetric shedding behaviour. For intermediate cavitation numbers, where cavity lengths vary up to 2 sphere diameters, there is a coupling or interaction between shed clouds and growing sheet cavities where two dominant frequencies are present in the wavelet power spectra. As the cavitation number is decreased, cavity lengths become greater making the period for sheet cavity growth and effect of the re-entrant jet greater and thus reducing the dominant frequencies. There appears to be a limiting cavitation number (and hence cavity length) where the re-entrant jet predominates resulting in a single dominant shedding frequency. At lower cavitation numbers, cavity lengths increase sufficiently that re-entrant jet fluid is generally swept downstream only occasionally reaching the forming sheet to affect break up.

Conclusions

The unsteady flow in the wake of a cavitating sphere differs fundamentally from that in single-phase flow. The collapse of circumferential cavities by the re-entrant jet phenomenon provides a new mechanism of periodic vortex shedding that allows large scale Karman-type horseshoe vortex structures to persist at Reynolds numbers spanning the whole supercritical range for single-phase flow. These large-scale vortex structures may rotate in a similar manner to that observed in single-phase flow, due to the asymmetric nature of the cavity collapse and the associated circumferential movement of the localised re-entrant jet.

High frequency periodicity characteristic of Kelvin-Helmholtz instability in the separating laminar shear layer is also evident from undulations in the interfacial layer at the edge of the cavity. The observed frequencies are in good agreement with those for maximum wave amplification. However, the absolute velocities of these disturbances are significantly higher than in single phase flow – evidently due to acceleration of the interfacial layer by viscous forces in the liquid that greatly exceed counteracting forces applied by the gaseous matter in the cavity.

The small-scale Kelvin-Helmholtz instability leads to rapid transition of the separated shear layer, with consequent irregular perturbation of the interfacial layer that leads to entrainment of small gas/vapour pockets and contributes to bubble cloud formation. Cavitation bubbles may also form as a result of low pressures in larger scale vortex cores.

The present investigation shows the need for more resolution of the cavitation number to gain further insight into the changing shedding regimes. Higher resolution high-speed photographic observations are also required to further investigate the behaviour of the interfacial layer at cavity separation.

Acknowledgments

The authors wish to acknowledge the assistance of Mr Bryce Pearce in carrying out experiments and the support of the DSTO, AMC and UTas.

References

- [1] Achenbach, E., Experiments on the Flow Past Spheres at Very High Reynolds Numbers, *J. Fluid Mech.*, 54, 1972, 565-575.
- [2] Addison, P. S. *The Illustrated Wavelet Transform Handbook*, Taylor & Francis, 2002.
- [3] Bakić, V. and Perić, M., Visualization of Flow Around a Sphere for Reynolds Numbers Between 22 000 and 400 000, *Thermophysics and Aeromechanics*, 12 2005, 307-315.
- [4] Brandner, P.A. Clarke, D.B. and Walker, G.J., *Development of a Fast Response Pressure Probe for Use in a Cavitation Tunnel*, Proceedings of the Fifteenth Australasian Fluid Mechanics Conference, Sydney, New South Wales, Dec, 2004, 4pp, (on CD).
- [5] Brennen, C.E., *Cavitation and Bubble Dynamics*, Oxford University Press, 1995.
- [6] Fage, A., Experiments on a Sphere at Critical Reynolds Numbers, *Aero. Res. Council*, London, R&M 1766, 1936.
- [7] Farge, M., Wavelet Transforms and Their Applications to Turbulence, *Annu. Rev. Fluid Mech.*, 24, 1992, 395-457.
- [8] Franc, J.P., *Partial Cavity Instabilities and Re-entrant Jet*, International Symposium on Cavitation CAV2001, Pasadena, USA, 2001.
- [9] Franc J. P. & Michel, J. M., *Fundamentals of Cavitation*, Kluwer Academic Publishers, 2004
- [10] Ho, C. M. and Huerre, P., Perturbed Free Shear Layers, *Ann. Rev. Fluid Mech.*, 16, 1984, 365-424.
- [11] Jaffard, S, Meyer, Y, and Ryan, R.D., *Wavelets, Tools for Science and Engineering*, SIAM, 2001.
- [12] Kjeldsen, M and Arndt, R.E.A, *Joint Time Frequency Analysis Techniques: A Study of Transitional Dynamics in Sheet/cloud Cavitation*, International Symposium on Cavitation CAV2003, Osaka, Japan, 2003.
- [13] Mørch, K.A., Bark, G., Grekula, M., Jønck, K.M., Nielsen, P.L. and Stendys, P., *The Formation of Cavity Clusters at Sheet Cavity/Re-entrant Jet Contact*, International Symposium on Cavitation CAV2003, Osaka, Japan, 2003.
- [14] Reisman, G.E. Wang, Y.-E. and Brennen C.E., Observations of Shock Waves in Cloud Cavitation, *J. Fluid Mech.*, 355, 1998, 255-283.
- [15] Schnerr, G. H., Schmidt, S., Sezal, I. and Thalhamer, M., *Shock and Wave Dynamics of Compressible Liquid flows with Special Emphasis on Unsteady Load on Hydrofoils and on Cavitation in Injection Nozzles*, International Symposium on Cavitation CAV2006, Wageningen, Netherlands, 2006.
- [16] Torrence, C. and Compo, G. P., A Practical Guide to Wavelet Analysis, *Bulletin of the American Meteorological Society*, 79, No.1, 1998, 61-78.